Nanoscale

PAPER

View Article Online
View Journal | View Issue

Cite this: *Nanoscale*, 2019, **11**, 19520

Cell membrane based biomimetic nanocomposites for targeted therapy of drug resistant EGFR-mutated lung cancer†

Pengying Wu,[a,b] Dongtao Yin,[c,d] Jiaming Liu,[a] Huige Zhou,[a] Mengyu Guo,[a] Jing Liu,[a,e] Yang Liu,[c] Xiaobing Wang,*[b] Ying Liu*[a] and Chunying Chen*[a]

Received 8th July 2019,
Accepted 20th September 2019

DOI: 10.1039/c9nr05791a

rsc.li/nanoscale

The therapeutic efficacy of anti-cancer nanomedicines is generally constrained due to limited accumulation in the solid tumors. In this study, we developed a biomimetic nano-carrier to enhance the chemotherapeutic efficacy of doxorubicin and icotinib in a chemo-resistant non-small cell lung cancer (NSCLC) cell line harboring a mutation in the epidermal growth factor receptor (EGFR). The unique nanomedicine was prepared by coating with targeting cancer cell membrane proteins as highly specific ligands. The resulting biomimetic nanoparticles were highly stable and exhibited superior homologous targeting ability *in vitro* compared with control groups. In a mouse EGFR-mutated NSCLC xenograft model, intravenous injection of the biomimetic nanomedicine led to a high tumour inhibition rate (87.56%). Histopathological analysis demonstrated that the biomimetic nanomedicine had minimal side effects. Taken together, a cancer cell membrane-based biomimetic drug carrier can significantly enhance drug accumulation and improve therapeutic efficacy in cancers.

Introduction

Lung cancer is associated with high morbidity, and is the leading cause of cancer-related deaths worldwide.[1] Non-small cell lung cancer (NSCLC) is the most common subtype of lung cancer, accounting for 85% of all lung tumours.[2] NSCLC patients harboring the L858R or exon 19 deletion mutations in the epidermal growth factor receptor (EGFR) benefit from EGFR tyrosine kinase inhibitors (EGFR-TKIs) like icotinib,[3] which was approved as the first-line therapy for advanced NSCLC cases with sensitive mutations in 2011 by the China Food and Drug Administration.[4] The efficacy and safety of icotinib in patients carrying EGFR mutations was also demonstrated in a Phase IV trial.[5] However, a secondary EGFR T790 M mutation often develops in patients after EGFR-TKI treatment, resulting in chemo-resistant tumors.[6] Therefore, it necessary to develop other strategies to treat NSCLC patients with the EGFR T790 M mutation, in order to improve therapeutic efficacy, and reduce the dosage and side effects of the chemotherapeutic drugs.

Nanotechnology has revolutionized the field of onco-therapeutics, especially in the development of drug delivery platforms. Drug-loaded nanoparticles like liposomes, polymers and dendrimers have achieved prolonged systemic circulation, sustained release and superior tumor penetration of the drugs.[7–9] Despite the tendency to passively accumulate at tumor sites *via* the enhanced permeability and retention (EPR) effect,[10,11] most nanoscale drug delivery systems showed poor circulation, tumor-site accumulation and penetration into the tumor interstitium in clinical trials.[12] This was attributed to the tumor microenvironment, which may present physical or biochemical barriers to the nanodrugs.[13] Therefore, nanoparticles were designed with surface-embedded ligands, such as transferrin, folic acid, enzymes, engineered antibodies and macromolecules (*e.g.* proteins and carbohydrates), which enabled tumor cell targeting.[14–16] These ligands have high specificity for tumor cell-specific receptors, which increases the uptake of the nano-carriers into tumor tissue.[17] However, the surface density of these ligands requires optimization to avoid recognition by the reticuloendothelial system, as well as

[a]*CAS Key Laboratory for Biomedical Effects of Nanomaterials and Nanosafety & CAS Center for Excellence in Nanoscience, National Center for Nanoscience and Technology of China, Beijing 100190, China. E-mail: chenchy@nanoctr.cn, liuy@nanoctr.cn*
[b]*Key Laboratory of Medicinal Resources and Natural Pharmaceutical Chemistry, Ministry of Education, College of Life Sciences, Shaanxi Normal University, Xi'an, Shaanxi, 710119, China. E-mail: wangxiaobing@snnu.edu.cn*
[c]*Department of Thoracic Surgery, General Hospital of the Chinese People's Liberation Army, Beijing, 100853, China*
[d]*Department of Thoracic Surgery, Rocket Force Characteristic Medical Center of the Chinese People's Liberation Army, Beijing, 100088, China*
[e]*The College of Life Sciences, Northwest University, Xi'an 710069, China*
†Electronic supplementary information (ESI) available. See DOI: 10.1039/c9nr05791a

interaction with serum proteins, in order to prolong circulation of the nanoparticles.[18] Biomimetic nanoengineering is a promising strategy that can overcome these concerns by modifying the nanoparticle surfaces with cell membranes from platelets, red-blood cells, leukocytes and mesenchymal-stem-cells.[19–23] Cancer cell-membrane vesicles contain surface proteins from the parent cells, which can enable the nanoparticles to home to the target cells through homotypic binding.[24,25]

Here, we developed cancer cell membrane protein-based biomimetic nanoparticles to overcome drug resistance in EGFR-mutant NSCLC cell lines. First, the cancer cell membrane (M) based nanoparticles were designed to target tumour cells *via* specific homotypic binding proteins, which can avoid the complicated procedure of modification with targeting molecules. Second, Poly (amidoamine) (PAMAM)-COOH (PC) dendrimers were synthesised, due to the strong side effects of PAMAM, and then icotinib (I) loaded into the PC dendrimers (I-PC). Subsequently, a commonly used anticancer drug, doxorubicin (Dox, D), was loaded to form the DI-PC nanoparticles by electrostatic adherence. Third, due to the small size of DI-PC (<10 nm), it can easily clear from the blood; therefore, we used a double emulsion method to synthesise PLGA (P) coated DI-PC nanoparticles (Fig. 1). As so far as we know, our design provides a convenient strategy to endow biomimetic drug carriers, this kind of strategy might be used as a common method for actively targeting nanoparticle-based drug combination to overcome drug resistance.

Methods

Isolation and characterization of cell membranes

The human NSCLC cell line HCC 827, the EGFR-TKI resistant lung cancer cell line H1975 that harbors an activating L858R mutation in exon 21 and a T790 M mutation in exon 20, and the mouse melanoma cell line B16 were purchased from the American Type Culture Collection (ATCC, Manassas, VA). All cell lines were cultured in RPMI 1640 medium supplemented with 10% fetal bovine serum (FBS), 1% penicillin–streptomycin, and 1% sodium pyruvate at 37 °C in a humidified incubator containing 5% CO_2. The plasma membranes of H1975 cells were isolated as previously described.[26] Briefly, the cells were harvested and re-suspended in ice-cold Tris-magnesium buffer (pH 7.4, 0.01 M Tris and 0.001 M $MgCl_2$) at the density of 1×10^8 cells per ml, and disrupted by extruding 20 times through a mini-extruder (Avanti, LF-1, Canada) without a polycarbonate membrane. The resulting homogenate was mixed with 1 M sucrose to dilute the latter to 0.25 M, and centrifuged at 2000*g* (4 °C, 10 min). The supernatant was collected and centrifuged again at 13 000*g* (4 °C, 30 min) to collect the cell membranes, which were then washed with ice-cold Tris-magnesium buffer containing 0.25 M sucrose, and collected after a second round of centrifugation. The proteins in the purified cell membranes were quantified using the bicinchoninic acid (BCA) protein assay kit (Pierce), and resolved by sodium dodecyl sulphate polyacrylamide gel electrophoresis (SDS-PAGE). The protein bands were transferred onto nitrocellulose membranes

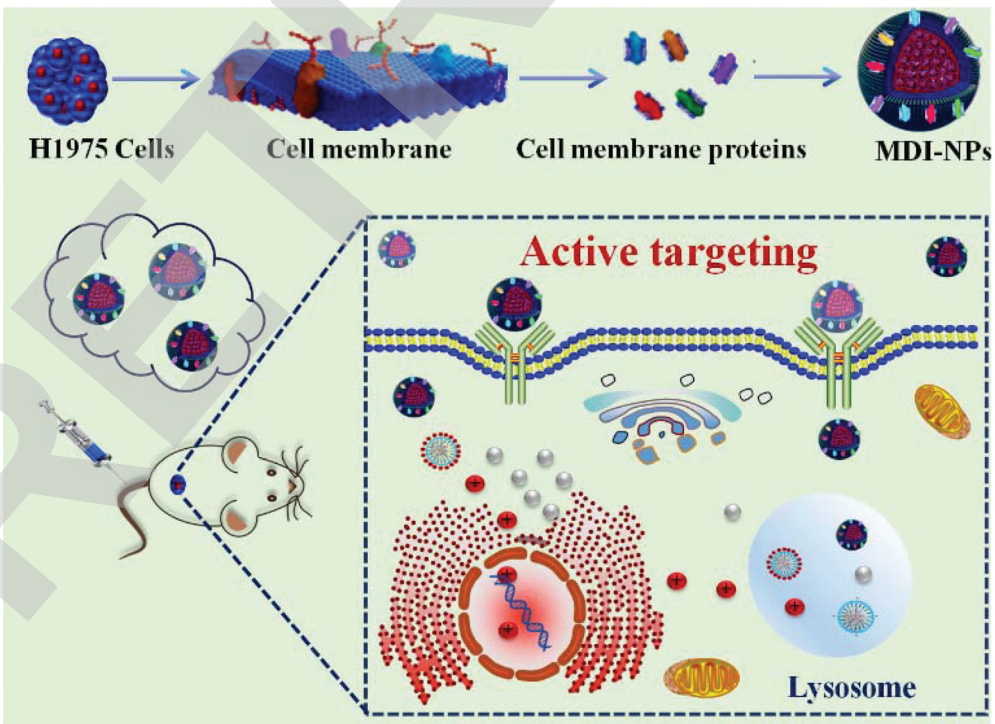

Fig. 1 Schematic illustration of the cancer cell membrane protein-based biomimetic nanoparticle, MDI, designed to overcome EGFR mutation targeting drug resistance.

(Millipore, Burlington, MA, USA), and incubated with anti-Na+/K+-ATPase, anti-Pan-cadherin, anti-Histone H3 and anti-COX IV primary antibodies (Cell Signaling). Following incubation with secondary antibodies (ZSGB-BIO), the positive bands were visualized using an enhanced chemiluminescence kit (Thermo Fisher Scientific, Rockford, USA).

Synthesis of cancer cell membrane-coated nanocomposites

PAMAM-COOH dendrimers (PC) were synthesized as our previously described.[27] A mixture of PC (10 mg dissolved in 4 ml deionized water) and icotinib (3 mg dissolved in 1 ml dichloromethane) was prepared, and sonicated for 5 min (200 W) with 1 s pulse and 2 s off. The solution was evaporated to remove the dichloromethane, and centrifuged in Microsep columns (MWCO: 30 kDa) to obtain the I-PC. The Dox-adsorbed I-PC (DI-PC) was subsequently prepared by adding 1 mg ml^{-1} Dox solution to I-PC, stirring the mixture overnight and centrifuging in the Microsep columns (MWCO: 30 kDa). To synthesize PLGA-coated nanocomposites (PDI-PC), 40 mg PLGA was dissolved in 2 mL dichloromethane by vortexing for 15 min. Once PLGA was completely dissolved, 500 μL DI-PC (W1) was added to the PLGA solution (O), and the mixture sonicated for 3 min to form a water in oil emulsion (W1/O). The latter was mixed with an 8 mL solution of 1% (w/w) PVA and 1% F68 (v/v = 1 : 1) (W2), and sonicated for 5 min as described above to form a double emulsion (W1/O/W2). After evaporating the W1/O/W2 emulsion to remove dichloromethane, the PLGA-coated nanocomposites were collected by centrifugation (10 000*g*, 10 min), and washed thrice with deionized water. The H1975 membrane protein-decorated PLGA nanocomposites (MDI) were fabricated by the extrusion method. Briefly, the cell membrane vesicles were extruded through polycarbonate membranes (400 nm) about 20 passes. Then, the vesicles were mixed with PLGA nanocomposites and extruded through polycarbonate membranes (200 nm) to obtain the membrane-coated nanoparticles.

Characterization of nanocomposites

The hydrodynamic diameter and zeta-potential of the nanocomposites were measured using a Malvern Zeta sizer Nano ZS instrument (Malvern Instruments, UK). Transmission electron microscopy (TEM) images were obtained using FEI Tecnai G2 F20 U-TWIN TEM (FEI Company, USA). Dox concentration was evaluated in terms of the absorbance at 480 nm using a spectrophotometer, in order to calculate the drug loading content. Icotinib concentration was similarly determined at 340 nm. Drug loading efficiency and entrapment efficiency were calculated using the following equations:

$$\text{Drug loading efficiency} = (\text{weight of drug in MDI})/(\text{weight of MDI})$$

$$\text{Drug entrapment efficiency} = (\text{weight of drug in MDI})/(\text{initial weight of drug})$$

The MDI particles were stored at 37 °C in different concentrations of FBS for 24 h, and their size was monitored to assess bio-stability. The average size and zeta potential were also detected after storage in PBS (pH 7.4) for one week to determine the stability of the MDI. The drug release from the nanoparticles at different pH was measured by dialysis against PBS.

In vitro cytotoxicity of MDI

The viability of H1975 cells exposed to the free and encapsulated drugs was measured using the cell counting Kit-8 (CCK-8) assay. Briefly, the cells were seeded into 96-well culture plates at the density of 1×10^4 cells per well and cultured for 24 h. Different concentrations of the reagents were added and after varying incubation periods, the culture medium was removed and replaced with serum-free medium containing 10 μL CCK-8 reagent. The cells were incubated further for 2 h at 37 °C, and the optical densities were measured at 450 nm on a microplate reader (SpectraMax M2MDC, USA). Calcin-AM and PI double staining was also performed to distinguish between live and dead cells by fluorescence microscopy.

Homotypic targeting of cancer cells

The cancer cell-targeting ability of the biomimetic nanoparticles was evaluated in terms of the cellular uptake of MDI and the spontaneous fluorescence of Dox. Briefly, the H1975 cells were seeded in 6-well plates and after a 24 h culture, incubated with different type of cell membrane coated nanoparticles at a 5 μM Dox for 6 h. The cellular uptake of nanoparticles was then determined by measuring the absorbance at 488 nm, and by confocal laser scanning microscopy (CLSM). In addition, the cells were harvested using trypsin, and washed thrice with cold PBS, and flow cytometry was used to quantify the intracellular fluorescence intensity.

Establishment of xenograft tumors and treatment regimen

Six-to-eight-week-old female BALB/c nude mice were housed in a temperature-controlled, ventilated and standard disinfected room. All animal experiments were conducted as per the protocols of the Institutional Animal Care and Use Committee at the Institute of Tumors of the Chinese Academy of Medical Sciences. The mice were subcutaneously injected in their hind leg with 1×10^6 H1975 cells. Once the tumors grew to approximately 50 mm^3, the mice were randomized into seven groups (n = 4 each) and intravenously injected with: (1) 100 μL of PBS, (2) 1 mg Dox per kg body weight, (3) 10 mg Icotinib per kg body weight, (4) I-NPs equivalent to 10 mg kg^{-1} Icotinib, (5) D-NPs equivalent to 1 mg Dox per kg, (6) DI-NPs equivalent to 10 mg kg^{-1} Icotinib and 1 mg kg^{-1} Dox, and (7) MDI equivalent to 10 mg kg^{-1} Icotinib and 1 mg kg^{-1} Dox. The reagents were injected every 2 days, and the tumor growth and body weight were monitored for the next 25 days. The mice were sacrificed after the 25th day, and the tumors were dissected and weighed. Blood samples were collected, left undisturbed at room temperature for 3 h, and centrifuged at 3000*g* for 15 min. The sera were aspirated and tested using a biochemical autoanalyser. The major organs (heart, liver, spleen, lung, and kidney) were also harvested, fixed in 10% formalin solu-

tion, embedded in paraffin and stained with hematoxylin–eosin (HE) as per standard protocols.

Statistical analysis

All data are presented as means ± SD of three independent experiments. Two-tailed Student's *t*-test was used to compare groups, and *p* values less than 0.05 were considered statistically significant.

Results and discussion

Synthesis and characterization of MDI

We successfully extracted and purified membrane proteins from a human lung cancer cell line as per our previously described protocol (extraction yield 0.98 mg per 1×10^8 cells), and embedded them in Dox and icotinib-loaded PLGA nanocomposites to form stable biomimetic particles (Fig. 2A). Dynamic light scattering analysis showed that the average hydrodynamic diameter of the MDI particles and PLGA nanocomposites were 157.5 ± 2.45 nm and 124.2 ± 1.10 nm respectively (Fig. 2B and C), which corresponds to the embedded proteins in the former. Furthermore, TEM imaging of MDI nanoparticles revealed a core/shell structure, along with a bright protein corona on the outer layer of PLGA (Fig. 2D). The protein profile of the MDI particles was next analyzed, and was consistent with that of H1975 cell membranes (Fig. 2E). The membrane-specific Na+/K+-ATPase and Pan-cadherin were detected, whereas the nuclear histone H3 and the mitochondrial COX IV were absent, indicating that only the membrane proteins were embedded on the surface of these nanoparticles. The zeta value of the membrane vesicles was approximately −35.7 mV, while that for MDI was −29.6 mV (Fig. 2F). The diameter and zeta potential of MDI nanoparticles were not observed significant changes after being stored in 1640 medium with different concentrations of FBS (pH 7.4) (Fig. 2H) or PBS (pH 7.4) for 7 days (Fig. S1†), indicating good stability of the MDI nanoparticles.

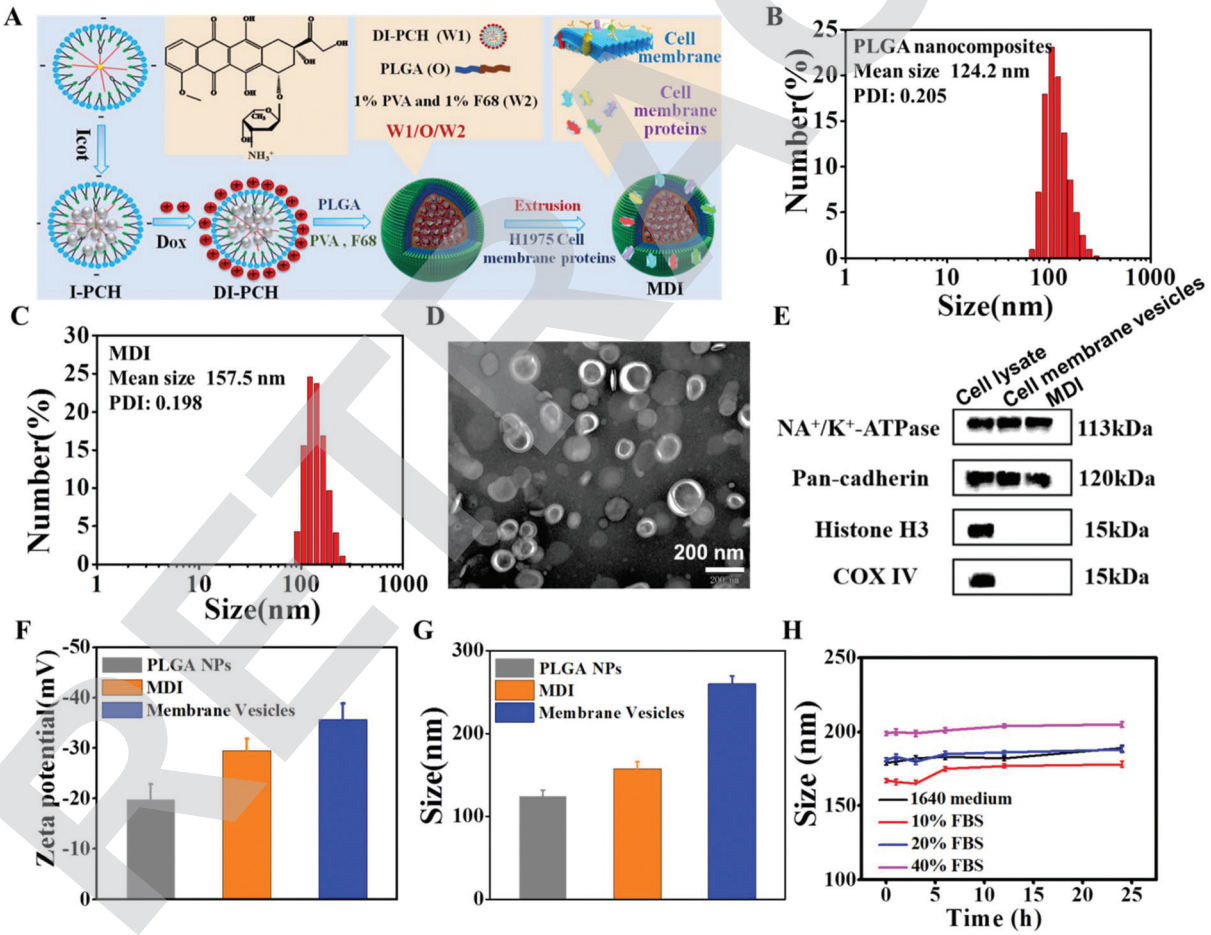

Fig. 2 Characteristics of cancer cell membrane coated NPs. (A) Schematic illustration of a cancer cell membrane protein-based biomimetic nanoparticle. (B) Dynamic light scattering analysis of PLGA nano-composites showing an average size distribution around 124 nm. (C) Dynamic light scattering analysis of MDI showing an average size distribution around 157 nm. (D) TEM image of MDI; scale bar, 200 nm. (E) Western blotting analysis of membrane-specific and intracellular protein markers. (F and G) Zeta potential and sizes of PLGA NPs, MDI, and membrane vesicles. Data expressed as means ± SD of three experiments. (H) Changes in diameter distributions of MDI after different storage times at 37 °C in medium containing different concentrations of FBS. Data are expressed as mean ± SD from three experiments.

Cell membrane protein coating retards drug release from the nanoparticles

The controlled drug release profiles are shown in Fig. 3A and B. At the physiological pH 7.4, only 30.1% of the Dox and 27.3% of icotinib were released from MDI within 48 h, indicating that the cell membrane proteins can suppress rapid Dox release in the bloodstream. However, a lower pH of 5 increased the amount of Dox released from the MDI particles, which is highly conducive for targeted drug release in

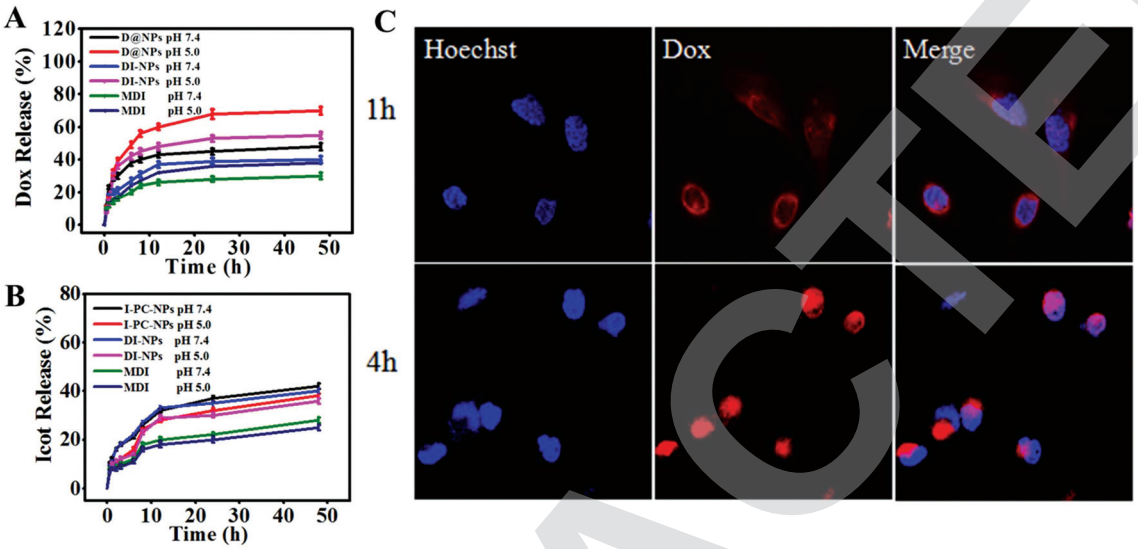

Fig. 3 Drug release study. (A) *In vitro* drug release of Dox from nanoparticles in PBS at different pH. (B) *In vitro* drug release profiles of icotinib from nanoparticles in PBS at different pH values. (C) Intracellular delivery of MDI in H1975 cells for 1 and 4 h. Cells were incubated with MDI at a Dox concentration of 5 μM and then observed by confocal microscopy.

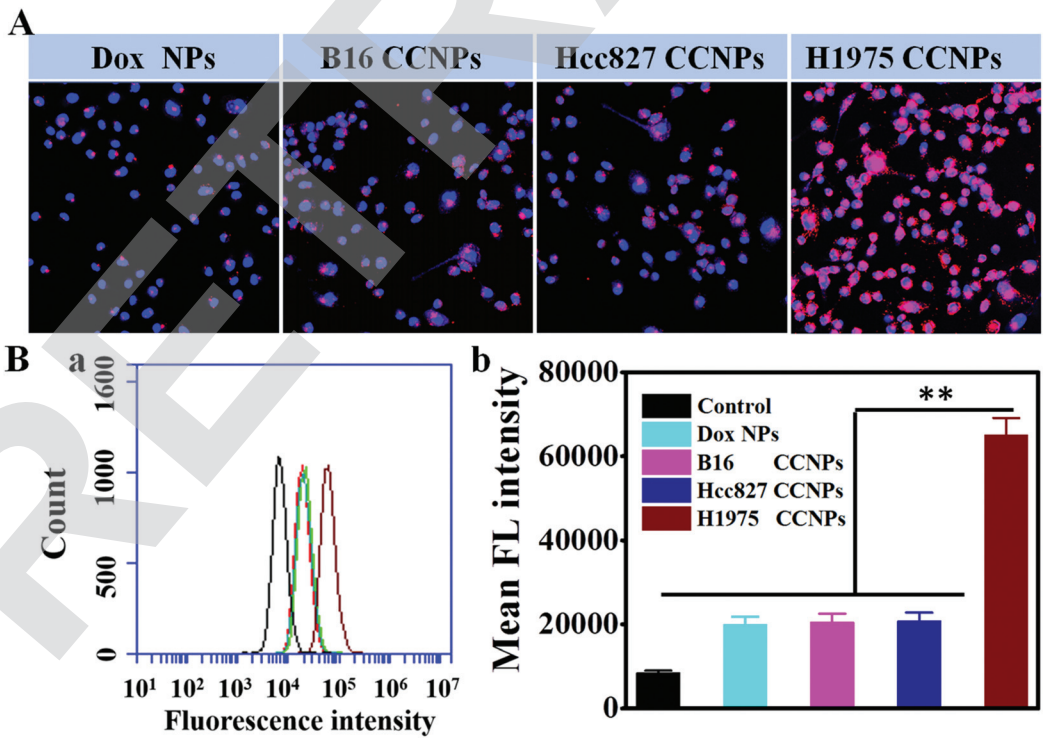

Fig. 4 MDI as a homotypically targeted delivery vehicle. (A) Fluorescent imaging of H1975 cells cultured with D-NPs, B16-NPs, HCC 827-NPs, and MDI. (Ba) Flow cytometric analysis of H1975 cells incubated with D-NPs, B16-NPs, HCC 827-NPs, and MDI. (Bb) Quantification of the mean fluorescence intensities of the histograms in (Ba). $^{**}p < 0.01$ compared with other groups.

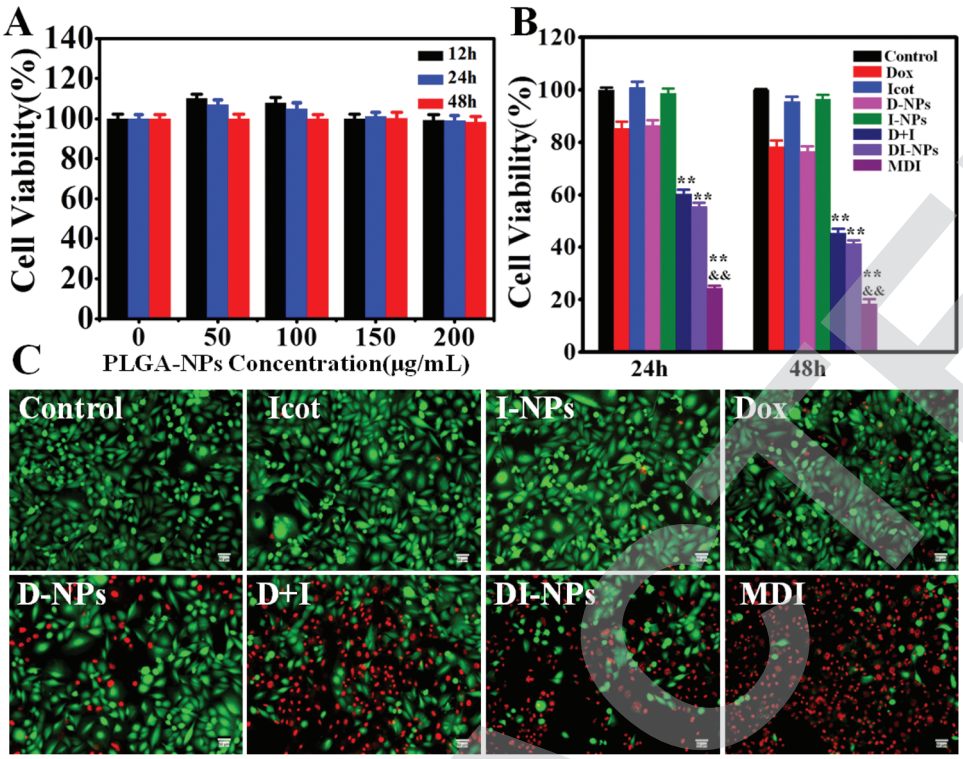

Fig. 5 Cell cytotoxicity. (A) Cell cytotoxicity of nanoparticles without Dox or icotinib after cultured for different times at different concentrations. (B) Cell cytotoxicity of different nanoparticles after cultured for 24 h and 48 h. $^{**}p < 0.01$ and $^{\&\&}p < 0.01$ compared with the control group. (C) Live-dead staining of H1975 cells after cultured for 48 h.

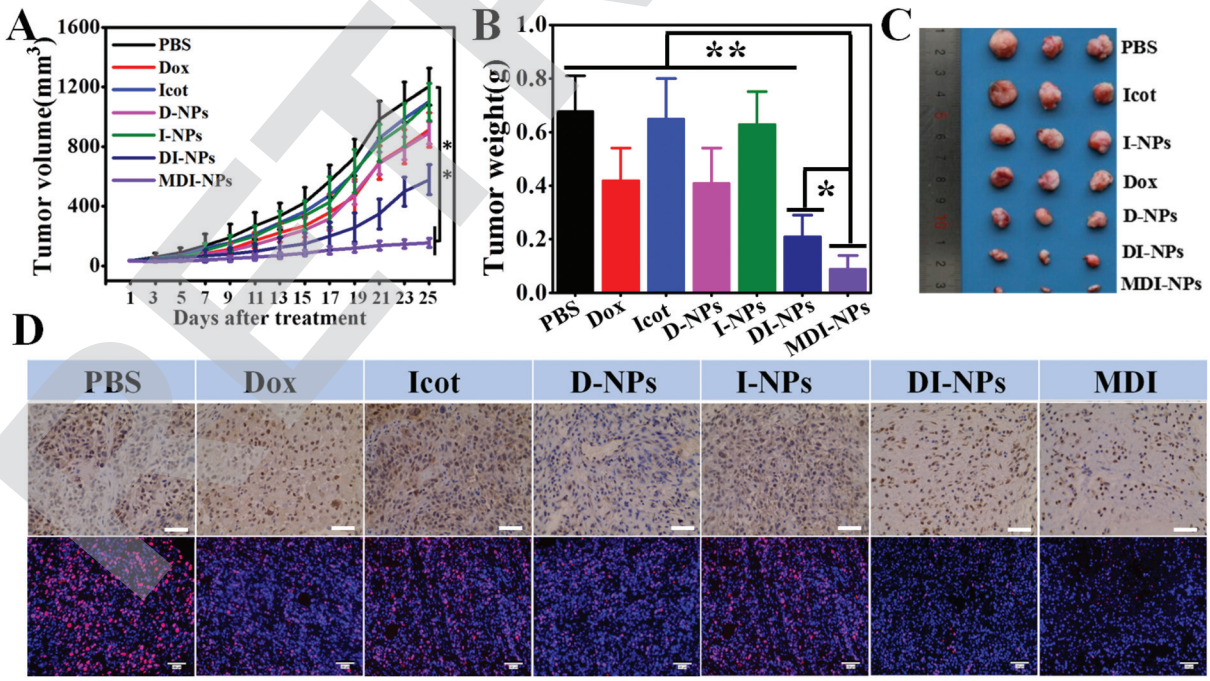

Fig. 6 *In vivo* tumor therapy. (A) Tumor volume growth curves. $^{**}p < 0.01$ compared with the PBS group. (B) Average weights of tumors collected from the mice at the end of treatment. $^{**}p < 0.01$ between the groups, $^{*}p < 0.05$ compared with DI-NPs groups. (C) Representative photographs of tumors at the end of treatment. (D) PCNA expression level (upper) and Ki67 immunofluorescence in tumor sections (lower). Scale bar = 50 nm.

the acidic tumor microenvironment and in the endo-lysosomes of tumor cells. Nevertheless, both Dox and icotinib were released relatively slowly from the nanoparticles regardless of the pH, indicating that the majority of drug molecules would likely remain encapsulated during circulation in the bloodstream, and thus reduce systemic toxicity. The intracellular localization of MDI was tracked using the red fluorescence of Dox. As shown in Fig. 3C, after both 1 and 4 h of incubation with MDI particles, Dox was primarily localized in the cytoplasm of the H1975 cells. This clearly indicated that once the nanoparticles entered the cells, Dox as released slowly into the cytoplasm and thenceforth entered the nuclei.

MDI biomimetic particles specifically target homotypic cells

Surface antigens mediate homologous adhesion of cancer cells, which is the rationale behind using cancer cell membrane-cloaked platforms to target cancer cells.[28–30] To evaluate the homotypic targeting ability of MDI to the H1975 cells, we incubated them with MDI-NPs (H1975 CCNPs), D-NPs, B16 cell membrane-coated nanoparticles (B16 CCNPs) and Hcc827 cell membrane coated nanoparticles (Hcc827 CCNPs), and observed significantly higher uptake of MDI compared to other nanoparticles (Fig. 4A and B). Taken together, the coating with H1975 cell membrane proteins endowed MDI with a strong homotypic targeting ability.

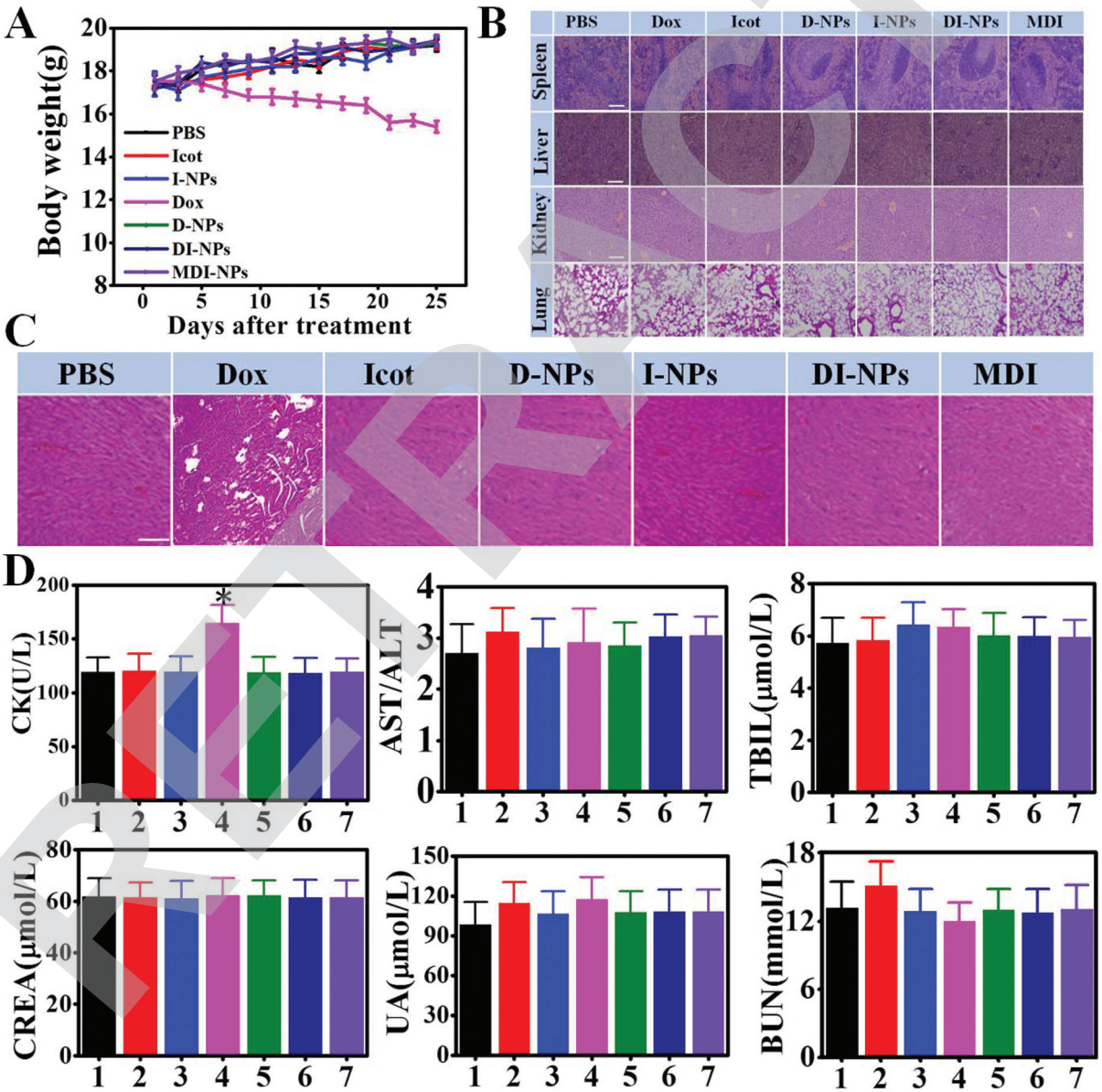

Fig. 7 Safety evaluation. (A) Body weight. (B) H&E staining of the major organs (Lung, Kidney, Liver and Spleen). Scale bar = 100 nm. (C) H&E staining of the hearts. Scale bar = 100 nm. (D) Blood biochemical analysis (1: PBS, 2: Icot, 3: I-NPs, 4: Dox, 5: D-NPs, 6: DI-NPs, 7: MDI). *$p < 0.05$ compared with the control group.

Biomimetic modification enhanced cytotoxicity of the chemotherapeutic drugs

The effect of the free and encapsulated drugs on the proliferation of H1975 cells was determined by CCK-8 assay. As shown in Fig. S2,† while even high doses of free icotinib only slightly inhibited proliferation of these cells, Dox clearly showed a dose-dependent cytotoxic effect. Based on these results, we incubated the H1975 cells with the different nanoparticles equivalent to 0.1 μM Dox and 10 μM icotinib. After 24 h incubation, D-NPs, I-NPs, DI-NPs and MDI decreased the cell viability to 84%, 98%, 57% and 25% respectively. The viability of cells incubated with MDI dropped further to 17% after 48 h, indicating a synergistic effect of Dox and icotinib, especially when encapsulated in biomimetic nanoparticles (Fig. 5B). In contrast, the nanoparticles without drug did not affect cell viability and have a good biocompatibility (Fig. 5A). The H1975 cells were stained with Calcien AM and propidium iodide (PI) to identify live and dead/apoptotic cells after the different treatments. As shown in Fig. 5C, icotinib or I-NPs barely affected cell viability, and only a few red-stained dead cells were seen following incubation with Dox and D-NPs. In contrast, DI-NPs induced significant cell death, and MDI markedly increased the proportion dead cells over the green-stained live cells. Taken together, biomimetic encapsulation can significantly amplify the synergistic toxicity of Dox and icotinib.

MDI nanoparticles effectively inhibit tumor growth *in vivo*

We also evaluated the *in vivo* therapeutic effects of the free drugs and different nanoparticle formulations in a H1975 tumor-bearing nude mice. During the 25-day treatment period, the body weight and tumor volume of the mice were monitored, following which the animals were sacrificed and their organs were analyzed. The tumor growth rate as significantly faster in the icotinib and I-NPs-treated groups (Fig. 6A), while free Dox and D-NPs achieved only a slight inhibition (21.45% and 25.67% respectively). Consistent with the *in vitro* results, the DI-NPs demonstrated significant tumor inhibition relative to D-NPs and I-NPs, indicating a synergistic effect on tumor regression and the ability to overcome drug resistance *in vivo*. The H1975 cell membrane-coated DI-NPs resulted in 87.56% tumor inhibition, with the tumor weight 8.75-fold less compared to that of the PBS control group. Furthermore, IHC analysis of the tumor tissues from the different groups showed significantly lower *in situ* expression levels of both PCNA and Ki67 in the MDI-treated compared to the other groups (Fig. 6D), clearly demonstrating inhibition of tumor proliferation. Taken together, the biomimetic PLGA nanocomposites with homotypic targeting ability have significant anti-tumor efficacy against resistant lung tumors.

Safety evaluation

Although the exact mechanism of Dox action in tumor cells is not completely understood, it is known that Dox intercalates into DNA, disrupts replication and transcription, and leads to cell death.[31] Despite its efficacy and broad clinical indications, Dox also causes severe side effects, including hepatotoxicity, cardiotoxicity and nephrotoxicity.[32,33] Therefore, we loaded Dox into nanoscale PAMAM dendrimers, which are extensively used to increase drug dispersion and reduce systemic toxicity. While free Dox resulted in considerable weight loss, none of the other treatment modalities affected the body weight of the mice (Fig. 7A). In addition, none of the mice exhibited any abnormal behavior during the entire treatment period (Fig. 7A). Histopathological examination of the major organs showed swelling of cardiac muscle fibers in the Dox-treated mice, while no visible heart damage was detected in the other groups (Fig. 7B). In addition, biochemical assessment of the sera demonstrated a significant increase in creatine kinase in the Dox-treated compared to the other groups, which is also indicative of cardiotoxicity (Fig. 7C). The encapsulation of Dox in the D-NPs, DI-NPs and MDI significantly reduced its systemic toxicity due to the tumor-specific accumulation and release of these nanoparticles. Finally, no pathological changes were observed in the liver, spleen, lung and kidney, and no aberrations were observed in the serum levels of hepatic or renal function markers in any of the groups (Fig. 7D). Taken together, MDI is an excellent therapeutic platform for precision cancer therapy mainly on account of its homotypic cancer cell targeting and excellent biocompatibility.

Conclusions

We developed a H1975 (T790M) cell membrane protein-based biomimetic nanomedicine to overcome drug resistance in NSCLC cells and achieve high drug accumulation in solid tumors. The cancer cell membrane protein coat improved homotypic cellular uptake and significantly inhibited tumor growth *in vivo* without any obvious side effects. This novel biomimetic nanoplatform is a highly promising tool for targeted cancer therapy.

Conflicts of interest

There are no conflicts to declare.

Acknowledgements

This work was financially supported by the National Science Fund for Excellent Young Scholars (31622026), the Key Program for International S&T Cooperation Projects of China (2016YFE0133100), the Science Fund for Creative Research Groups of the National Natural Science Foundation of China (11621505), the National Natural Science Foundation of China (21876205, 11435002, 91543206) and the National Basic Research Program of China (2017YFC1600204, 2016YFA0201600, and 2016YFA0203204).

Notes and references

1 R. L. Siegel, K. D. Miller and A. Jemal, *CA Cancer J. Clin.*, 2016, **66**, 7–30.
2 S. Xu, S. K. Lam, P. N. Cheng and J. C. Ho, *Cancer Sci.*, 2018, **109**, 3471–3482.
3 L. Wang, Y. Li, L. Li, Z. Wu, D. Yang, H. Ma and D. Wang, *OncoTargets Ther.*, 2018, **11**, 2345–2353.
4 J. Wang, Y. Wang, C. Zheng, K. Hou, T. Zhang, X. Qu, Y. Liu, J. Kang, X. Hu and X. Che, *Cell Biol. Int.*, 2018, **42**, 1292–1299.
5 X. Hu, B. Han, A. Gu, Y. Zhang, S. C. Jiao, C. L. Wang, J. He, X. Jia, L. Zhang, J. Peng, M. Wu, K. Ying, J. Wang, K. Ma, S. Zhang, C. You, F. Tan, Y. Wang, L. Ding and Y. Sun, *Lung Cancer*, 2014, **86**, 207–212.
6 Y. Wang, Y. Wei, X. Ma, X. Ma and P. Gong, *Medicine*, 2018, **97**, e11346.
7 J. Shi, P. W. Kantoff, R. Wooster and O. C. Farokhzad, *Nat. Rev. Cancer*, 2017, **17**, 20–37.
8 R. K. Jain and T. Stylianopoulos, *Nat. Rev. Clin Oncol.*, 2010, **7**, 653–664.
9 L. Jin, X. Zeng, M. Liu, Y. Deng and N. He, *Theranostics*, 2014, **4**, 240–255.
10 S. K. Golombek, J. N. May, B. Theek, L. Appold, N. Drude, F. Kiessling and T. Lammers, *Adv. Drug Delivery Rev.*, 2018, **130**, 17–38.
11 D. H. Yang, H. J. Kim, K. Park, J. K. Kim and H. J. Chun, *Drug Delivery*, 2018, **25**, 950–960.
12 X. Wang, F. Yan, X. Liu, P. Wang, S. Shan, Y. Sun, Z. Sheng, Q. Liu, J. F. Lovell and H. Zheng, *J. Controlled Release*, 2018, **286**, 358–368.
13 J. Wang, J. Liu, Y. Liu, L. Wang, M. Cao, Y. Ji, X. Wu, Y. Xu, B. Bai, Q. Miao, C. Chen and Y. Zhao, *Adv. Mater.*, 2016, **28**, 8950–8958.
14 Z. Yang, S. Jiang, F. Li, Y. Qiu, J. Gu, R. I. Pettigrew, M. Ferrari, D. J. Hamilton and Z. Li, *Angew. Chem., Int. Ed.*, 2019, **58**, 5272–5276.
15 D. R. Elias, A. Poloukhtine, V. Popik and A. Tsourkas, *Nanomedicine*, 2013, **9**, 194–201.
16 Y. Z. Du, L. L. Cai, J. Li, M. D. Zhao, F. Y. Chen, H. Yuan and F. Q. Hu, *Int. J. Nanomed.*, 2011, **6**, 1559–1568.
17 M. Zhu, X. Ding, R. Zhao, X. Liu, H. Shen, C. Cai, M. Ferrari, H. Y. Wang and R. F. Wang, *J. Controlled Release*, 2018, **28**, 72–82.
18 R. H. Fang, C. M. Hu, B. T. Luk, W. Gao, J. A. Copp, Y. Tai, D. E. O'Connor and L. Zhang, *Nano Lett.*, 2014, **14**, 2181–2188.
19 R. H. Fang, A. V. Kroll, W. Gao and L. Zhang, *Adv. Mater.*, 2018, **30**, 1706759.
20 Y. Jia, Z. Sheng, D. Hu, F. Yan, M. Zhu, G. Gao, P. Wang, X. Liu, X. Wang and H. Zheng, *Biomater. Sci.*, 2018, **6**, 1546–1555.
21 H. Sun, J. Su, Q. Meng, Q. Yin, L. Chen, W. Gu, P. Zhang, Z. Zhang, H. Yu, S. Wang and Y. Li, *Adv. Mater.*, 2016, **28**, 9581–9588.
22 C. Liu, D. Wang, S. Zhang, Y. Cheng, F. Yang, Y. Xing, T. Xu, H. Dong and X. Zhang, *ACS Nano*, 2019, **13**, 4267–4277.
23 W. Liu, M. Zou, T. Liu, J. Zeng, X. Li, W. Yu, C. Li, J. Ye, W. Song, J. Feng and X. Zhang, *Adv. Mater.*, 2019, **31**, e1900499.
24 L. Rao, L. Bu, B. Cai, J. Xu, A. Li, W. Zhang, Z. Sun, S. Guo, W. Liu, T. Wang and X. Zhao, *Adv. Mater.*, 2016, **28**, 3460–3466.
25 H. Sun, J. Su, Q. Meng, L. Chen, W. Gu, Z. Zhang, H. Yu, P. Zhang, S. Wang and Y. Li, *Adv. Funct. Mater.*, 2017, **27**, 1604300.
26 Y. Jia, X. Wang, D. Hu, P. Wang, Q. Liu, X. Zhang, J. Jiang, X. Liu, Z. Sheng, B. Liu and H. Zheng, *ACS Nano*, 2019, **13**, 386–398.
27 J. Tang, H. Zhou, X. Hou, L. Wang, Y. Li, Y. Pang, C. Chen, G. Jiang and Y. Liu, *Cancer Lett.*, 2018, **423**, 16–26.
28 B. T. Luk and L. Zhang, *J. Controlled Release*, 2015, **220**, 600–607.
29 J. Y. Zhu, D. W. Zheng, M. K. Zhang, W. Y. Yu, W. X. Qiu, J. J. Hu, J. Feng and X. Z. Zhang, *Nano Lett.*, 2016, **16**, 5895–5901.
30 S. Y. Li, H. Cheng, B. R. Xie, W. X. Qiu, J. Y. Zeng, C. X. Li, S. S. Wan, L. Zhang, W. Liu and X. Zhang, *ACS Nano*, 2017, **11**, 7006–7018.
31 M. Cagel, E. Grotz, E. Bernabeu, M. A. Moretton and D. A. Chiappetta, *Drug Discovery Today*, 2017, **22**, 270–281.
32 T. O. Omobowale, A. A. Oyagbemi, U. E. Ajufo, O. A. Adejumobi, O. E. Ola-Davies, A. A. Adedapo and M. A. Yakubu, *J. Diet. Suppl.*, 2018, **15**, 183–196.
33 K. Nagai, A. Oda and H. Konishi, *Food Chem. Toxicol.*, 2015, **78**, 147–152.